Novel Readout Scheme for MEMS Vibratory Gyroscopes Based on Signal Phase Shift

M. Dalal, A. N. Shirazi, W. K. Sung, G. Casinovi and F. Ayazi

Abstract

This paper introduces and demonstrates experimentally a new readout scheme for MEMS vibratory gyroscopes that relies on signal phase instead of signal amplitude to measure the rotation rate. When the drive and sense resonance modes of the gyroscope are both excited by forces of equal intensity and 90° phase difference, the Coriolis force induces a phase shift in the gyroscope response that is proportional to the gyroscope rotation rate. This effect is predicted by theoretical analysis and has been verified through simulation and measurement of two different gyroscopes, a high-frequency bulk acoustic wave (BAW) disk gyroscope, and a low-frequency mode-matched tuning fork gyroscope (M2-TFG). The two gyroscopes report a measured phase sensitivity of 0.597 mV/°/s and 0.148 mV/°/s, respectively. The linear response observed on both devices supports the use of the phase readout architecture as a valid measurement scheme.

Copyright Notice

NOVEL READOUT SCHEME FOR MEMS VIBRATORY GYROSCOPES BASED ON SIGNAL PHASE SHIFT

M. Dalal[*], A.N. Shirazi, W.K. Sung, G. Casinovi, and F. Ayazi
Georgia Institute of Technology, Atlanta, Georgia, USA

ABSTRACT

This paper introduces and demonstrates experimentally a new readout scheme for MEMS vibratory gyroscopes that relies on signal phase instead of signal amplitude to measure the rotation rate. When the drive and sense resonance modes of the gyroscope are both excited by forces of equal intensity and 90° phase difference, the Coriolis force induces a phase shift in the gyroscope response that is proportional to the gyroscope rotation rate. This effect is predicted by theoretical analysis and has been verified through simulation and measurement of two different gyroscopes, a high-frequency bulk acoustic wave (BAW) disk gyroscope, and a low-frequency mode-matched tuning fork gyroscope (M^2-TFG). The two gyroscopes report a measured phase sensitivity of 0.597 mV/°/s and 0.148 mV/°/s, respectively. The linear response observed on both devices supports the use of the phase readout architecture as a valid measurement scheme.

INTRODUCTION

The most common readout architectures currently implemented in Coriolis-based MEMS vibratory gyroscopes rely on signal amplitude to measure the rotation rate of the device. In this type of readout scheme, only one of two resonance modes of the device is electrically excited. The Coriolis force caused by a rotation around the gyroscope axis creates a coupling between the two modes, so that the amplitude of the second resonance mode – which is used as the sense signal – is proportional to the angular velocity of rotation Ω_z [1].

This paper introduces a new method of measuring the gyroscope rotation rate based on signal phase instead of signal amplitude. In this scheme, the drive and sense resonance modes are both excited by forces that are of equal intensity but 90° out of phase. A theoretical analysis of a 2-DOF mass-spring gyroscope model [2] shows that the Coriolis force induces a phase shift in the responses of the two resonance modes of the gyroscopes. For sufficiently small rotation rates, the phase shift is proportional to the angular velocity of rotation Ω_z. Therefore, it can be used to measure the gyroscope rotation rate using standard phase-detection circuitry.

A phase-based readout scheme offers several advantages over the more traditional amplitude-based methods mentioned earlier. First, the amplitude of the output signal remains constant, thus minimizing the effect of additive noise. More importantly, it can be shown that a rotating excitation induces a similar phase shift in the responses of the two resonance modes, thus mimicking the effect of physical rotation [2]. This fact can be exploited to devise self-calibrating gyroscope architectures that do not require the addition of any moving parts to the gyroscope assembly.

THEORETICAL ANALYSIS

The analysis that follows examines the effect of the Coriolis force on the response of a mode-matched vibratory gyroscope ($f_{drive} = f_{sense} = \omega_0/2\pi$) when excitations 90° out of phase with one another are applied to the two resonance modes of the device with matched frequencies. In this paper, these modes will be designated as I and Q, respectively. It is assumed that the gyroscope rotates around its z-axis (the sensitive axis) at a constant angular velocity Ω_z with respect to a fixed inertial frame of reference. Then the

behavior of the gyroscope can be analyzed in terms of its normal mode model, which consists of an n equivalent 2-DOF mass-spring system, is described by the following set of equations

$$\ddot{x} + \frac{\omega_0}{Q}\dot{x} - 2\lambda\Omega_z\dot{y} + \omega_0^2 x = F_1\cos(\omega_0 t)$$
$$\ddot{y} + \frac{\omega_0}{Q}\dot{y} - 2\lambda\Omega_z\dot{x} + \omega_0^2 y = F_2\sin(\omega_0 t) \qquad (1)$$

where x and y are generalized coordinates, ω_0 is the resonance frequency of the mass-spring system, Q the quality factor, and λ a constant that depends on the gyroscope type and on the index of the resonance mode of the device [3]. The steady-state solution to this set of differential equations can be found using phasor analysis, which transforms (1) into the following equivalent set of algebraic equations

$$j\omega_0\begin{bmatrix} \omega_0/Q & -2\lambda\Omega_z \\ 2\lambda\Omega_z & \omega_0/Q \end{bmatrix}\begin{bmatrix} X \\ Y \end{bmatrix} = \begin{bmatrix} F_1 \\ -jF_2 \end{bmatrix}$$

The solution to these equations is

$$X = \frac{1}{j\omega_0}\frac{(\omega_0/Q)F_1 - j2\lambda\Omega_z F_2}{(\omega_0/Q)^2 + (2\lambda\Omega_z)^2}$$
$$Y = -\frac{1}{j\omega_0}\frac{2\lambda\Omega_z F_1 + j(\omega_0/Q)F_2}{(\omega_0/Q)^2 + (2\lambda\Omega_z)^2}$$

which corresponds to the following sinusoidal functions

$$x(t) = \frac{Q}{\omega_0}\frac{\sqrt{(F_1\omega_0)^2 + (2F_2Q\lambda\Omega_z)^2}}{\omega_0^2 + (2Q\lambda\Omega_z)^2}\sin(\omega_0 t - \theta_1)$$
$$= A_1\sin(\omega_0 t - \theta_1)$$
$$y(t) = -\frac{Q}{\omega_0}\frac{\sqrt{(F_2\omega_0)^2 + (2F_1Q\lambda\Omega_z)^2}}{\omega_0^2 + (2Q\lambda\Omega_z)^2}\cos(\omega_0 t - \theta_2) \qquad (2)$$
$$= A_2\cos(\omega_0 t - \theta_2)$$

where

$$\theta_1 = \tan^{-1}\left(\frac{2F_2Q\lambda\Omega_z}{F_1\omega_0}\right), \quad \theta_2 = \tan^{-1}\left(\frac{2F_1Q\lambda\Omega_z}{F_2\omega_0}\right) \qquad (3)$$

The expressions in (2) are the steady-state solutions of (1), and it can be seen that the Coriolis force introduces phase shifts θ_1 and θ_2 in the gyroscope response. For small values of Ω_z, these phase shifts are directly proportional to Ω_z.
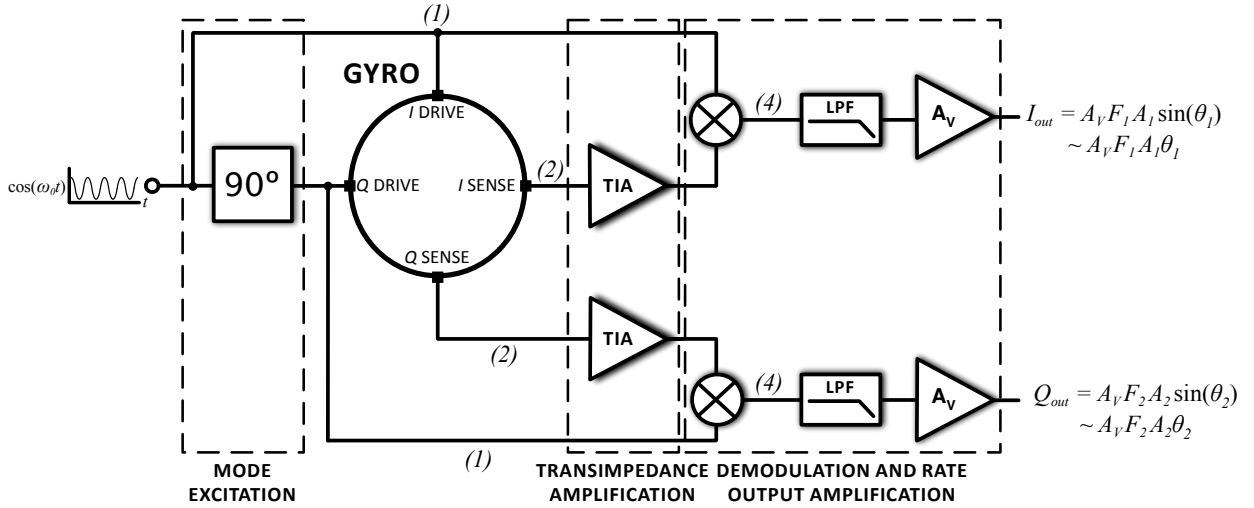
Figure 1: Block diagram of phase-shift readout architecture

A block diagram of the phase readout architecture is shown in Fig. 1, in which the drive forces from (1) are applied to the two degenerate resonance modes of the gyroscope through the electrodes identified as I_{Drive} and Q_{Drive}, respectively. The gyroscope responses in (2) are seen at output terminals I_{Sense} and Q_{Sense}, which are 90° out of phase with each other as well as their respective inputs. After a Coriolis excitation is applied to the z-axis, the drive and sense signals from each complementary mode are multiplied together, giving

$$I_{mult}(t) = F_1 A_1 \cos(\omega_0 t) \sin(\omega_0 t - \theta_1)$$
$$Q_{mult}(t) = F_2 A_2 \sin(\omega_0 t) \cos(\omega_0 t - \theta_2) \qquad (4)$$

where A_1 and A_2 are the coefficients of the sine and cosine terms in (2). Using trigonometric identities, the expressions in (4) simplify to

$$I_{mult}(t) = \frac{F_1 A_1}{2}\Big[\sin(2\omega_0 t - \theta_1) - \sin\theta_1\Big]$$
$$Q_{mult}(t) = \frac{F_2 A_2}{2}\Big[\sin(2\omega_0 t - \theta_2) + \sin\theta_2\Big] \qquad (5)$$

Following the low pass filtering and rate output amplification stages, the frequency components at $2\omega_0$ are removed from (5), reducing the signal of the phase readout scheme output to

$$I_{out}(t) = -\frac{F_1 A_1}{2}\sin\theta_1, \; Q_{out}(t) = \frac{F_2 A_2}{2}\sin\theta_2 \qquad (6)$$

in which $\sin\theta \approx \theta$ for small values of θ.

SIMULATION RESULTS

The linear relationship between phase shift in the gyroscope response and its rotation rate was verified using ANSYS numerical simulations of actual designs of a bulk acoustic wave (BAW) disk gyroscope [4,5] and a tuning fork gyroscope [6] (Fig. 2).

The BAW gyroscope consists of a center-supported disk structure fabricated on a [100] silicon wafer with capacitively-coupled drive, sense, and control electrodes. It operates in the in-
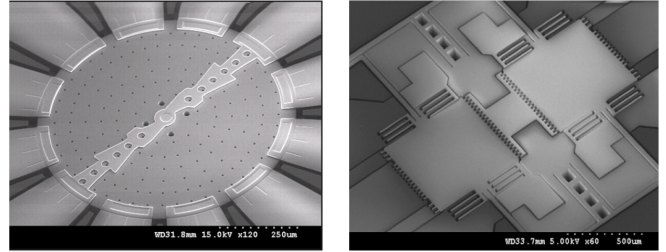

Figure 2: SEM of bulk acoustic wave (BAW) disk gyroscope (left) and tuning fork gyroscope (M^2-TFG, right)

plane resonance mode of index $n = 3$, ensuring that both the I and Q modes have the same resonance frequency (~10MHz) despite the anisotropic nature of single-crystal silicon [4]. Sinusoidal input excitations were applied to the drive electrodes aligned with one of the degenerate resonance modes (I_{Drive}), while excitations of equal amplitude but 90° out of phase were applied to the drive electrodes aligned with its complementary degenerate mode (Q_{Drive}). The phases of the output currents at all the electrodes obtained from finite element simulations were recorded at eight different rotation rates, ranging from zero to 2100 °/s (Fig. 3). The extracted scale factor sensitivity is 3.81×10^{-4} °/(°/s).
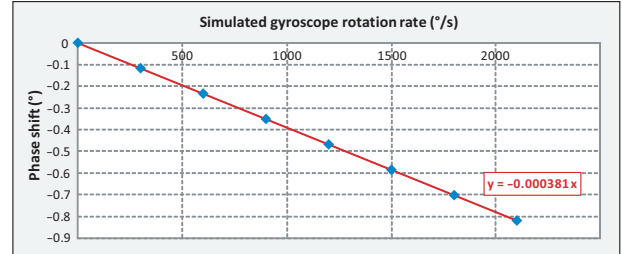

Figure 3: Simulated phase shift in the BAW disk gyroscope response due to Coriolis force, measured relative to its value at zero rotation rate. The solid line shows the theoretical analysis predictions from (3) assuming $F_1 = F_2$.

Similar ANSYS simulations were performed on a mode-matched tuning fork gyroscope (M^2-TFG), a device comprised of two proof masses supported by a network of flexural springs
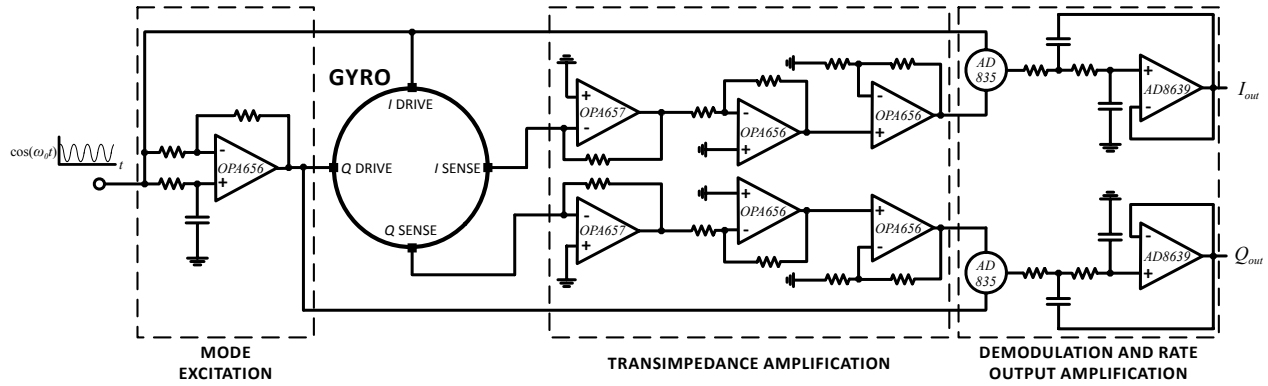
Figure 4: Schematic diagram of phase-shift interface electronics.

anchored to a central post with control electrodes symmetrically distributed around the proof masses [6]. The M^2-TFG can attain high quality factors because its large proof mass and optimized anchor and flexural mode design reduce device surface and support losses, as well as thermo-elastic damping. However, the large size and flexural actuation of the structure result in a resonance frequency almost 1000 times lower than that of the BAW disk gyroscope.

The results of the ANSYS simulations of the M^2-TFG are shown in Fig. 5. Along with Fig. 3, these results confirm that the phase shift is directly proportional to the rotation rate of the gyroscope. The simulated scale factor sensitivity of the M^2-TFG is 2.51 °/(°/s), while the equations in (3) with $F_1=F_2$ yield a value of 2.67 °/(°/s). This discrepancy can be explained by the fact that in our M^2-TFG design, the electrodes corresponding to the I mode have slightly different area from the electrodes corresponding to the Q mode.
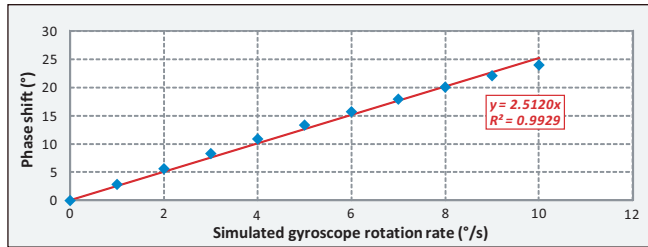

Figure 5: Simulated phase shift in the M^2-TFG response due to Coriolis force, measured relative to its value at zero rotation rate. The solid line shows the best linear fit to the data.

MEASURED RESULTS AND DISCUSSION

In order to validate the results of the theoretical analysis and numerical simulation experimentally, the phase shift readout architecture shown in Fig. 1 was implemented on a printed circuit board (PCB), the schematic of which is shown in Fig. 4. Separate PCBs were made for the BAW (Fig. 6) and M^2-TFG so that the unique footprints and traces of each device could be placed without adding too much complexity and size to the PCB design. In both cases, the input I-mode drive voltage was generated using an Agilent 4395A network analyzer locked into the resonance frequency of the respective device (ω_0). This signal was passed to both the gyroscope and an on-board tunable phase shifter that used a discrete op-amp (TI OPA656) to generate the 90° phase shift for the device Q-mode excitation signal.

On both the M^2-TFG and BAW PCBs, separate amplifier chains were used to read out the I-mode and Q-mode sense signals.

For the BAW, a trans-impedance amplifier (OPA657) was used at the sense channel input to provide current-to-voltage conversion and amplification of the phase-shifted signal. This signal was then passed to two voltage amplifiers that provided additional amplification and buffering for the mixer (AD835) stages. For the M^2-TFG, the input TIA was replaced with an OPA656, which provided higher gain and lower bandwidth than the OPA657. The remaining amplifiers on this board matched their counterpart on the BAW PCB; however, the gain and bandwidth of each stage was adjusted for use with a low-frequency gyroscope.
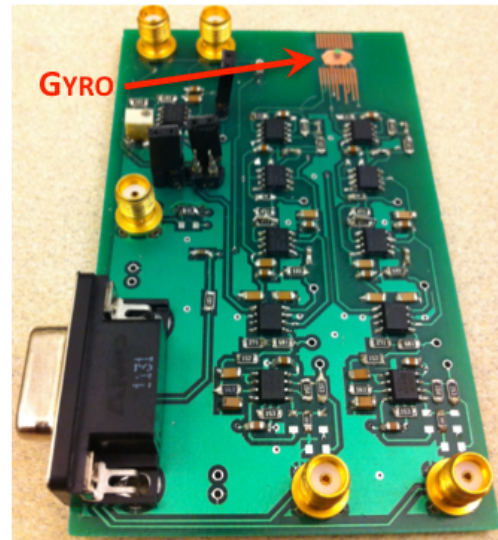

Figure 6: Phase readout PCB

For the BAW disk gyroscope, sinusoidally-varying rotation rates ranging from 0 to 10 °/s were applied via the rate table. Consequently, the output signals denoted as I_{out} and Q_{out} in Fig. 1 were also observed to be sinusoids with amplitudes proportional to the applied rotation rate (Fig. 7). At the applied rates, it was derived that θ_1 and θ_2 would remain small enough to satisfy equation (6).

The BAW gyroscope was tested with an input power of 0 dBm applied to the I_{Drive} and Q_{Drive} terminals of the device. An Ideal Aerosmith rate table was used to generate sinusoidally-varying rotation rates ranging from 0 to 10 °/s. The corresponding output signal (I_{out} in Fig. 4) is shown in Fig. 7. The measured datapoints were closely aligned along a straight line with a slope of

0.6 mV/°/s (Fig. 8). The linearity of the collected measurements confirms the response predicted by the theoretical calculations and numerical simulations.
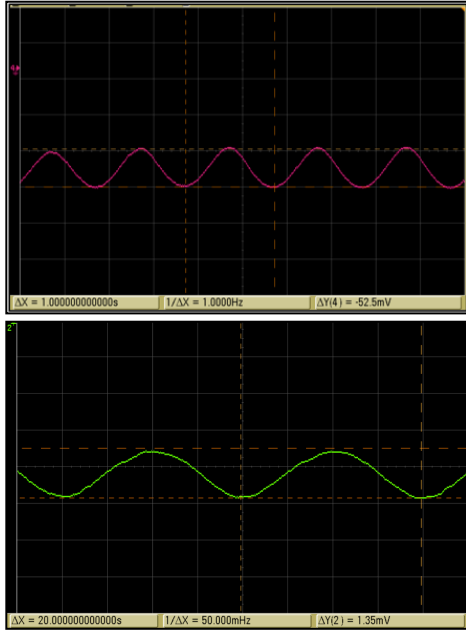

Figure 7: Oscilloscope traces of (top) BAW gyroscope output (I_{out}) and (bottom) M^2-TFG gyroscope output (I_{out}) at 50 °/s and 8 °/s, respectively.

Measurements were also taken on the M^2-TFG using applied rotation rates from 0 to 10 °/s (Fig. 7); however, the applied input power was reduced to -4 dBm to prevent the device from saturating. The scale factor measurements (Fig. 8) show a device sensitivity 0.15 mV/°/s. Like the BAW gyroscope, the M^2-TFG also exhibits a very linear response to the input excitation.

Table 1 summarizes the simulated and measured performance parameters of both gyroscopes.
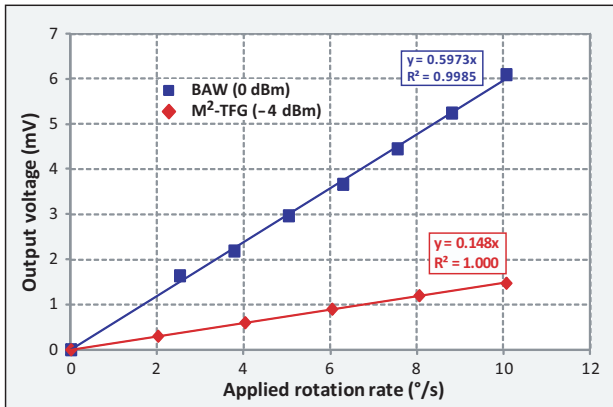

Figure 8: Measured phase shift response due to Coriolis force for the BAW and tuning fork gyroscopes, respectively, relative to its value at zero rotation rate. Each solid line shows the best linear fit to the data.

CONCLUSIONS

The simulation results and experimental measurements described in the previous sections confirm that the phase-shift readout scheme introduced in this paper is an effective method of measuring the rotation rate of both high-frequency (BAW) and low-frequency (M^2-TFG) gyroscopes. In principle, this readout scheme can be applied to any gyroscope that can be modeled by a 2-DOF mass-spring system. As mentioned in [2], the phase readout scheme can be integrated with a calibration scheme that does not require the use of a rotary stage for proper operation. However, the tradeoffs between amplitude- and phase-based readout schemes must be more thoroughly analyzed for a more robust comparison of the two systems and their benefits and challenges.

Table 1: Phase-shift readout performance summary of BAW and M^2-TFG gyroscopes

	BAW	**M^2-TFG**
	SIMULATION	
Q (simulated)	20,000	50,000
f_0 (simulated)	10 *MHz*	5.95 *kHz*
Phase-Sensitivity	3.81×10^{-4} °/(°/s)	2.51 °/(°/s)
	MEASUREMENT	
Q	32,000	60,000
f_0	9.65 *MHz*	11.7 *kHz*
Excitation Power	0 *dBm*	-4 *dBm*
Phase Sensitivity	0.597 *mV/(°/s)*	0.148 *mV/(°/s)*

ACKNOWLEDGEMENTS

REFERENCES

[1] F. Ayazi and K. Najafi, "A HARPSS Polysilicon Vibrating Ring Gyroscope," J. Microelectromech. Syst., 10, 2 (2001).

[2] G. Casinovi, W.K. Sung, M. Dalal, A.N. Shirazi, and F. Ayazi, "Electrostatic Self-Calibration of Vibratory Gyroscopes," IEEE International Conference on Micro Electro Mechanical Systems, Paris, France (2012), pp. 559–562.

[3] B.J. Gallacher, J.S. Burdess, A.J. Harris, and M.E. McNie, "Principles of a Three-Axis Vibrating Gyroscope," IEEE Trans. Aerosp. Electron. Syst., 37, 4 (2001).

[4] H. Johari and F. Ayazi, "Capacitive Bulk Acoustic Wave Silicon Disk Gyroscopes," IEEE International Electron Devices Meeting, San Francisco, USA (2006), pp. 513–516.

[5] W.K. Sung, M. Dalal, and F. Ayazi, "A 3MHz Spoke Gyroscope with Wide Bandwidth and Large Dynamic Range," IEEE International Conference on Micro Electro Mechanical Systems, Hong Kong (2010), pp. 104–107.

[6] M.F. Zaman, A. Sharma, Z. Hao, and F. Ayazi, "A Mode-Matched Silicon-Yaw Tuning-Fork Gyroscope with Subdegree-Per-Hour Allan Deviation Bias Instability," J. Microelectromech. Syst., 17, 6 (2008).

CONTACT

*M. Dalal, tel: +1-404-385-3291; mdalal@gatech.edu